CHEMISTRY
A EUROPEAN JOURNAL

DOI: 10.1002/chem.200700885

The Electronic Structure of the Tris(ethylene) Complexes [M(C_2H_4)$_3$] (M = Ni, Pd, and Pt): A Combined Experimental and Theoretical Study

Nicole Hebben,[a] Hans-Jörg Himmel,*[b] Georg Eickerling,[c] Carmen Herrmann,[c] Markus Reiher,*[c] Verena Herz,[d] Manuel Presnitz,[d] and Wolfgang Scherer*[d]

Abstract: In this article we analyze in detail the electronic properties of the D_{3h}-symmetric tris(ethylene) complexes of nickel, palladium, and platinum ([M(C_2H_4)$_3$] M = Ni, Pd, Pt). In the case of [Pd(C_2H_4)$_3$] the analysis is based on new experimental IR and Raman spectra for the matrix-isolated molecules and in all cases on the results of quantum-chemical (DFT) calculations. The experimental spectra collected for [Pd(C_2H_4)$_3$] provide evidence for several previously unobserved vibrational modes, including the in-phase and out-of-phase ν(C–C) and δ(CH_2) modes, and the in-phase ν(M–C) mode. Special consideration is given to possible inter-ligand interactions. The interaction force constant $f_{CC,CC}$ between two C_2H_4 ligands can be directly estimated from the spectra, and its very small value (0.002 N m^{-1}) indicates the absence of any significant inter-ligand interaction. An analysis of the topology of the theoretical electron density distribution, $\rho(\mathbf{r})$, and the corresponding Laplacian, $\nabla^2\rho(\mathbf{r})$, for [Pd(C_2H_4)$_3$] and its lighter and heavier homologues [Ni(C_2H_4)$_3$] and [Pt(C_2H_4)$_3$], respectively, is in full agreement with the conclusions drawn from the experimental results. The combined experimental and quantum-chemical results provide detailed insights in the electronic properties of these prototypical ethylene complexes.

Keywords: density functional calculations · Group 10 elements · olefin complexes · palladium · vibrational spectroscopy

Introduction

Numerous authenticated examples of transition-metal ethylene complexes[1] are known today. Considerable focus has been placed on nickel complexes, because they represent key intermediates responsible for the "nickel effect". Whereas ethylene and triethylaluminum react under high pressure and at 100 °C to give exclusively trialkylaluminum compounds featuring long alkyl chains, the addition of small amounts of nickel(II) salts leads to the formation of butene. The synthesis of [Ni(C_2H_4)$_3$] was reported as early as 1973.[2] The molecule has been suggested to exhibit a D_{3h}-symmetric structure in which the nickel and all the carbon atoms are located in the same plane (called a "planar" structure). Much effort has been directed into the analysis of the detailed structure because the mechanism responsible for the nickel effect includes the formation of such a complex, which later forms a bond to trialkylaluminum, before undergoing an electrocyclic reorganization process. Quantum-chemical calculations have confirmed the "planar" structure.[3] A second possible structure, namely the D_{3h}-symmetric "upright" structure, in which the midpoints of the ethylene ligands and the Ni atom occupy one plane, is energetically disfavored by about 117 kJ mol^{-1} according to B3LYP[4] and by about 187 kJ mol^{-1} according to MP2[5] calculations. The order has been explained qualitatively on the basis of the Dewar–Chatt–Duncanson (DCD) model.[6] The σ bonds are expected to be of similar strength in both forms, but the π bonds should be stronger in the planar form. However,

[a] N. Hebben
Institut für Technische Chemie und Polymerchemie
Universität Karlsruhe
Engesserstrasse 20, 76131 Karlsruhe (Germany)

[b] Prof. Dr. H.-J. Himmel
Anorganisch-Chemisches Institut
Ruprecht-Karls-Universität Heidelberg
Im Neuenheimer Feld 270, 69120 Heidelberg (Germany)
Fax: (+49) 6221-54-5707
E-mail: hans-jorg.himmel@aci.uni-heidelberg.de

[c] Dr. G. Eickerling, Dr. C. Herrmann, Prof. Dr. M. Reiher
Laboratorium für Physikalische Chemie, ETH Zürich Hönggerberg,
Wolfgang-Pauli-Strasse 10, 8093 Zürich (Switzerland)
Fax: (+41) 44-63-31594
E-mail: markus.reiher@phys.chem.ethz.ch

[d] V. Herz, M. Presnitz, Prof. Dr. W. Scherer
Institut für Physik
Universität Augsburg, 86135 Augsburg (Germany)
Fax: (+49) 821-598-3227
E-mail: wolfgang.scherer@physik.uni-augsburg.de

the DCD model, although advantageous in providing straightforward answers, has been shown in many cases to be an oversimplification.[7] Many derivatives, including some for Pd and Pt, have been structurally characterized in subsequent years; for example, the crystal structure of tris-(bicyclo[2.2.1]heptene)platinum that features double-bonded C atoms and a Pd atom in one plane.[8] $[Pt(C_2H_4)_2(C_2F_4)]$ is another example, which has been structurally characterized and for which the planar geometry has been confirmed.[9] The Pt–C(F_2) and Pt–C(H_2) distances are 197 and 225 pm, respectively, and the C–C bond lengths are 144 and 136 pm for the coordinated C_2F_4 and C_2H_4 ligands, respectively, which are thus slightly longer than that in free C_2H_4 (131.3 pm[10]). Very recently, the isoelectronic $[Ag(C_2H_4)_3]^+$ ion was structurally characterized.[5] This ion was stabilized with the aid of the weakly coordinating anion $[Al\{OC(CF_3)_3\}_4]^-$ and represents yet another example of the "planar" structural type. However, the energy difference between the "planar" and "upright" form was estimated to be much smaller (44 kJ mol^{-1} according to MP2 calculations).

The interest in the properties of these benchmark compounds has been further stimulated by a recent paper in which it was suggested, on the basis of theoretical descriptors extracted from quantum-chemical calculations, that the C_2H_4 ligands in $[Ni(C_2H_4)_3]$ and also the C_2H_2 ligands in $[Ni(C_2H_2)_3]$ interact to a large extent, leading to homoaromaticity.[4] According to these authors, this effect accounts for the facile cyclization of the ligands. The obvious question arising before one can judge the importance of this potential interaction is how strong this interaction is. Unfortunately, the authors of reference [4] did not give a satisfactory answer to this question. From an experimentalist's point of view, the vibrational properties are of great importance to confirm or disprove such a hypothesis. A significant interaction between the C_2H_4 ligands must bring about a splitting between the in-phase and out-of-phase combinations of the C–C stretches, ν(C–C), coupled with the deformations $\delta(CH_2)$ and, most sensitively, the wagging modes $\omega(CH_2)$, due to the presence of significant interaction force constants (see Discussion). The matrix-isolated $[Ni(C_2H_4)_3]$ molecule has been studied in detail by using both IR[11] and Raman spectroscopy.[12] The inspection of the accumulated data, overlooked by the authors of the article[4] on the homoaromaticity of $[Ni(C_2H_4)_3]$, clearly shows that for all modes the interaction force constants are extremely weak, which would disfavor a homoaromatic effect. Reactions between Ni atoms and C_2H_2 yielded only $[Ni(C_2H_2)]$ and $[Ni(C_2H_2)_2]$, but not $[Ni(C_2H_2)_3]$.[13] Quantum-chemical calculations indicate that the unknown 1:3 complex should not be completely flat (leading to D_3 instead of D_{3h} symmetry) because of significant steric repulsion between the hydrogen atoms of adjacent C_2H_2 ligands.[4]

To further evaluate the electronic properties of this class of compounds, we have studied the IR and Raman spectra of the heavier homologue $[Pd(C_2H_4)_3]$ by using the matrix-isolation technique. The matrix-isolation technique offers not only the possibility to stabilize this molecule, but also has the advantage that the bands/signals in the vibrational spectra are sharp (rotations are quenched) and the interactions with the surrounding environment are only very weak, so that even small wavenumber differences between the modes can be easily monitored. The molecule has already been studied previously by using IR spectroscopy.[14] However, we present for the first time Raman spectra for $[Pd(C_2H_4)_3]$ and Raman and IR data for the perdeuterated isotopomer $[Pd(C_2D_4)_3]$. In addition to the experimental studies, quantum-chemical calculations were carried out, and all of the accumulated data allow a more detailed understanding of the electronic properties of this benchmark molecule. Special consideration is devoted to possible ligand–ligand interactions and comparisons with other related ethylene complexes. We then analyze and compare the electron density distribution in the three complexes $[Ni(C_2H_4)_3]$, $[Pd(C_2H_4)_3]$, and $[Pt(C_2H_4)_3]$.

Results and Discussion

We will first briefly discuss the structures of the tris-(ethylene) complexes $[M(C_2H_4)_3]$. Detailed information is already available. We then turn to our experimental vibrational study on $[Pd(C_2H_4)_3]$ carried out for the matrix-isolated molecule. Finally, the charge density distribution will be analyzed, providing detailed information about the bonding in these systems.

Structures of the tris(ethylene) complexes: Structural details for the tris(ethylene) complexes are already available from experimental (X-ray and neutron diffraction), as well as quantum-chemical studies. In the case of $[Pt(C_2H_4)_3]$, neutron diffraction data provide detailed insight into the structural properties.[15] This study gave the following bond lengths and bond angles: Pt–C 217.6(2), C–C 140.2(7), C–H 108.9(5) pm; Pt-C-C 71.2(1), C-C-H 121.2(4)/124.0(4), Pt-C-H 110.8(3)/107.5, H-C-H 111.5(4)°. The structural parameters obtained by our ZORA-BP86/I calculations (see Table 1) are in excellent agreement with the experimental results. Apart from the Pt–C bond length which differs by only 1.8 pm, the bond lengths and angles are reproduced within the experimental standard deviations.

Table 1. Calculated (ZORA-BP86/I) structural parameters (bond lengths [pm], bond angles [°]) for the tris(ethylene) complexes $[M(C_2H_4)_3]$ (M = Ni, Pd, Pt).

	$[Ni(C_2H_4)_3]$	$[Pd(C_2H_4)_3]$	$[Pt(C_2H_4)_3]$
C–C	139.4	138.9	140.6
C–H	109.1	109.0	109.0
M–C	204.3	222.2	219.4
C-M-C	39. 9	36.4	37.4
H-C-H	115.1	115.8	115.3
H-C-C	120.3	120.6	120.1

Vibrational analysis of matrix-isolated $[Pd(C_2H_4)_3]$: Although vibrational studies have already been reported for all $[M(C_2H_4)_3]$ complexes, we carried out a thorough vibrational (IR and Raman) study for $[Pd(C_2H_4)_3]$ isolated in Ar and in pure C_2H_4 matrices providing for the first time clear evidence for some important vibrational modes (see below), which were not reported in the previous studies. Figure 1

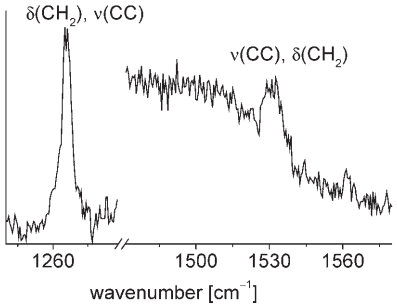

Figure 1. Raman spectrum obtained for $[Pd(C_2H_4)_3]$ in a pure C_2H_4 matrix, excited with the 488 nm line of an Ar^+ laser.

displays two characteristic regions of the Raman spectrum of a C_2H_4 matrix containing Pd, showing a strong signal at 1266 cm^{-1} and a much weaker one at 1531 cm^{-1}. On the basis of experiments with different concentrations of ethylene and Pd in the matrix and control experiments with N_2 and O_2, both signals can be assigned to $[Pd(C_2H_4)_3]$.[16] The Raman spectrum of the matrix-isolated homologue $[Ni(C_2H_4)_3]$ has been shown to contain signals in similar regions (at 1516 and 1242/1252 cm^{-1}).[12]

IR spectra of the matrix-isolated molecule were also recorded, although some of the IR bands had already been reported previously.[14] In our experiments, we used an Ar matrix containing 10% of C_2H_4 instead of a pure C_2H_4 matrix because the C_2H_4 bands dominate thus masking huge parts of the spectral region. Bands at 2920, 1525, and 1256 cm^{-1} appeared in the spectra generated by our experiments and were assigned to $[Pd(C_2H_4)_3]$. These wavenumbers are very close to those reported earlier (2918, 1524, and 1255 cm^{-1}).[14] An additional very weak band was detected at 903 cm^{-1} (904 cm^{-1} in the earlier work). Thus our IR results are in agreement with the earlier work. The wavenumber of the IR band near 1525 cm^{-1} is close to the signal at 1531 cm^{-1} in the Raman spectra, and the wavenumber of the band near 1255 cm^{-1} in the IR spectra is close to the signal at 1266 cm^{-1} in the Raman spectra. For comparison, these four features are plotted together in Figures 2 and 3. It will be shown later

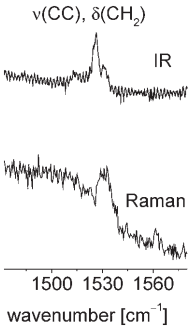

Figure 2. Comparison between the in-phase and out-of-phase ν(C–C), $\delta(CH_2)$ modes of $[Pd(C_2H_4)_3]$ at 1531 and 1525 cm^{-1} as observed in the Raman and IR spectra.

that the small energy differences provide useful information about possible ligand–ligand interactions.

The experiments were repeated, but this time with C_2D_4 in place of C_2H_4. In our Raman experiments, signals at 312 and 1385 cm^{-1} can be assigned to $[Pd(C_2D_4)_3]$ with certainty (see Figure 4). These positions are close to those reported for $[Ni(C_2D_4)_3]$ (344 and 1362 cm^{-1}), which were there assigned to the in-phase Ni–C and C–C stretching fundamentals.[12] IR spectra of the perdeuterated

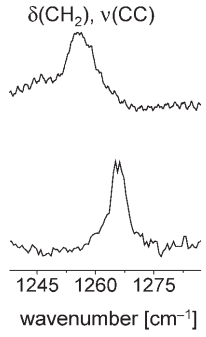

Figure 3. Comparison between the in-phase and out-of-phase $\delta(CH_2)$, ν(C–C) modes of $[Pd(C_2H_4)_3]$ at 1266 and 1256 cm^{-1} as observed in the Raman and IR spectra.

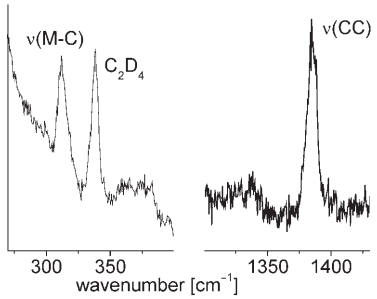

Figure 4. Raman spectrum obtained for $[Pd(C_2D_4)_3]$ in a pure C_2D_4 matrix, excited with the 488 nm line of an Ar^+ laser.

matrix-isolated $[Pd(C_2D_4)_3]$ have not yet been published. Our experiments gave evidence for a strong broad band at 1378 cm^{-1}, and another broad band at 951 cm^{-1}, which are both assignable to $[Pd(C_2D_4)_3]$. In the case of $[Ni(C_2D_4)_3]$, bands in similar regions (at 1362 and 952 cm^{-1}) were reported. Figure 5 shows the Raman signal at 1385 cm^{-1} together with the IR band at 1378 cm^{-1}. Again, the small energy difference between the two features is of significance for the following discussion.

There can now be no doubt that the tris(ethylene) complex of Pd exhibits D_{3h} symmetry (see above). The high symmetry is apparent from the fact that the strongest signals observed in the Raman spectra are absent in the IR spectra and vice versa. In D_{3h} symmetry, the vibrational fundamentals span the irreducible representations $5a_1' + 4a_2' + 10e' + 4a_1'' + 4a_2'' +$

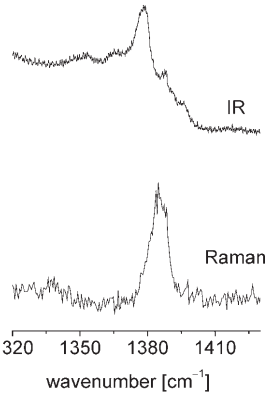

Figure 5. Comparison between the in-phase and out-of-phase ν(C–C) modes of $[Pd(C_2D_4)_3]$ as observed in the Raman and IR spectra.

$7e''$. Only the e' modes are both IR and Raman active. The a_1' and e'' modes are only Raman active, and the a_2'' modes are IR active only. The a_2' and a_1'' modes are both IR and Raman silent. With the help of the selection rules, the effect of isotopic substitution (H/D) and comparison with similar molecules, and by using the results of quantum-chemical calculations, we can assign the observed features in our spectra without difficulty. In Tables 2 and 3 the observed wavenumbers are compared to those calculated. It can be seen that the general level of agreement is very good. Our Raman experiments thus agreed with two of the five a_1' modes, namely the two modes with significant character from both the in-phase C–C stretch and CH_2 deformation at 1531 and 1266 cm^{-1} ($\nu_2(a_1')$ and $\nu_3(a_1')$, respectively). In our IR experiments, four of the ten e' modes were traced (at 2920, 1525, 1256, and 903 cm^{-1}), which can be described as out-of-phase combinations of C–H stretches ($\nu_{11}(e')$) and C–C stretches mixed with CH_2 deformations ($\nu_{12}(e')$ and $\nu_{14}(e')$).

A description of the molecular motions of these modes was not found to be straightforward. Hence it is well known that for free C_2H_4, the C–C stretch and CH_2 deformation of the same symmetry are heavily coupled, leading to a mode at 1623 cm^{-1} and another at 1342 cm^{-1}.[24] In C_2H_4 complexes, this mixing is expected to be even larger because the energetic difference between the two modes decreases. In this light, it has previously been pointed out that it is almost impossible to draw any conclusions about the bond properties just by inspection of the wavenumber shift upon coordination, because the degree of mode coupling varies from complex to complex. Table 4 includes the experimental wavenumbers of the two coupled ν(C–C) and $\delta(CH_2)$ modes for several complexes which have been studied by using the matrix-isolation technique or in solution. It includes the complexes $[Fe(C_2H_4)_2]$,[17] $[Co(C_2H_4)_n]$ ($n=1,2$),[18] $[Ni(C_2H_4)_n]$ ($n=1$[19] and 2[20]), $[Pd(C_2H_4)]$,[21] $[Pd(C_2H_4)_3]$, $[Pt(C_2H_4)_3]$,[35] $[Cu(C_2H_4)_n]$ ($n=1$–3),[22] $Ag(C_2H_4)$, and $Au(C_2H_4)$,[23] as well as the neutral main-group element complexes $[Li(C_2H_4)]$,[24] $[Al(C_2H_4)]$,[25] and $[In(C_2H_4)]$.[26] It should be mentioned that silacyclopropylidene, SiC_2H_4, has also been studied.[27] In this molecule the mode with the highest degree of ν(C–C) occurs at a wavenumber as low as 1011.9 cm^{-1}. However, the electronic situation within this molecule certainly differs significantly from that of all other species. Most of the vibrational information relies exclusively on IR studies, giving thus especially in the case of the D_{3h}-symmetric tris(ethylene) complexes, where not all modes are IR active, an incomplete set of vibrational data. Some of the complexes included in Table 4 have also been studied by methods other than vibrational spectroscopy. Thus, for example, EPR spectra are available for the matrix-isolated $[Cu(C_2H_4)_n]$ and $[Ag(C_2H_4)_n]$ complexes,[28] and the UV/Vis spectrum of $[Cu(C_2H_4)_n]$ has also been reported.[29] While most of the atoms have been observed to form stable π-bonded ethylene complexes, matrix experiments show that Ti atoms react further to give the two products $[H_2Ti(C_2H_2)]$ and $[HTi(C_2H_3)]$.[30] The wavenumbers from vibrational spectra recorded for $[Ni(C_2H_4)_3]$ and $[Pt(C_2H_4)_3]$ in petroleum ether solutions are also included in Table 4.[31]

The trends between the (calculated) bond lengths and observed wavenumbers of the C–C stretching modes as given in

Table 2. Comparison between observed and calculated (ZORA-BP86/I level of approximation) wavenumbers [cm^{-1}] for $[M(C_2H_4)_3]$ (M = Ni, Pd, and Pt) with IR intensities [km mol^{-1}] and the Raman activities [$Å^4$ amu^{-1}] of the calculated wavenumbers given in parentheses. Note that the experimental values refer exclusively to matrix-isolation experiments.

$[Ni(C_2H_4)_3]$			$[Pd(C_2H_4)_3]$			$[Pt(C_2H_4)_3]$	
IR	Raman	calcd	IR	Raman	calcd	calcd	Assigned
		3046.9 (0/741.1)			3059.6 (0/501.9)	3052.3 (0/661.4)	ν_1 (a_1')
	1516	1504.9 (0/14.9)		1531	1517.1 (0/41.5)	1497.9 (0/9.7)	ν_2 (a_1')
	1252	1240.0 (0/10.5)		1266	1250.0 (0/109.4)	1224.7 (0/88.4)	ν_3 (a_1')
	928	938.5 (0/7.8)			918.4 (0/3.8)	958.9 (0/10.7)	ν_4 (a_1')
	358	365.6 (0/25.3)			321.5 (0/32.9)	385.5 (0/30.5)	ν_5 (a_1')
		3033.8 (0/0)			3059.5 (0/0)	3043.0 (0/0)	ν_6 (a_2')
		1410.8 (0/0)			1416.5 (0/0)	1415.9 (0/0)	ν_7 (a_2')
		926.1 (0/0)			898.6 (0/0)	929.6 (0/0)	ν_8 (a_2')
		454.2 (0/0)			394.7 (0/0)	442.6 (0/0)	ν_9 (a_2')
		3044.8 (32.3/11.7)			3059.5 (7.1/0.5)	3052.5(21.8/1.9)	ν_{10} (e')
		3039.5 (47.2/162.8)	2920		3051.6 (41.6/78.3)	3046.4(57.7/153.2)	ν_{11} (e')
1512		1501.6 (28.5/15.5)	1525		1512.3 (18.2/46.6)	1492.5(7.6/27.2)	ν_{12} (e')
		1418.8 (5.4/11.4)			1420.8 (5.3/11.5)	1420.2(2.0/18.3)	ν_{13} (e')
1242		1238.8 (34.1/15.2)	1256		1246.9 (66.6/6.2)	1214.3(77.1/2.5)	ν_{14} (e')
917		937.2 (0.0/0.3)	903		911.2 (1.5/1.0)	946.1 (1.4/1.1)	ν_{15} (e')
		918.0 (4.0/5.1)			884.5 (15.7/5.6)	908.8 (2.6/6.1)	ν_{16} (e')
404		441.6 (10.8/8.6)			403.0 (0.6/13.0)	461.6 (0.3/21.0)	ν_{17} (e')
373		383.3 (53.0/5.9)			300.1 (36.2/0.7)	317.3 (31.8/4.3)	ν_{18} (e')
		221.1 (22.0/2.1)			146.3 (12.6/4.1)	136.7 (27.9/1.4)	ν_{19} (e')
		3101.7 (0/0)			3122.5 (0/0)	3115.1 (0/0)	ν_{20}(a_1'')
		1185.7 (0/0)			1185.9 (0/0)	1185.0 (0/0)	ν_{21} (a_1'')
		921.8 (0/0)			929.1 (0/0)	916.2 (0/0)	ν_{22} (a_1'')
		100.0 (0/0)			122.3 (0/0)	115.4 (0/0)	ν_{23} (a_1'')
		3132.6 (41.5/0)			3148.0 (21.3/0)	3140.0 (24.7/0)	ν_{24} (a_2'')
		818.3 (2.1/0)			807.9 (0.1/0)	809.2 (2.1/0)	ν_{25} (a_2'')
		668.6 (2.0/0)			607.6 (0.2/0)	691.8 (0.2/0)	ν_{26} (a_2'')
		208.5 (0.2/0)			138.2 (0.6/0)	155.8 (2.1/0)	ν_{27} (a_2'')
		3128.5 (0/237.5)			3146.8 (0/164.3)	3139.4 (0/222.5)	ν_{28} (e'')
		3106.1 (0/163.9)			3123.2 (0/184.0)	3116.0 (0/196.3)	ν_{29} (e'')
		1207.3 (0/0.3)			1199.6 (0/1.5)	1198.5 (0/1.3)	ν_{30} (e'')
		916.0 (0/4.3)			935.6 (0/0.6)	908.9 (0/0.2)	ν_{31} (e'')
		798.2 (0/1.3)			799.7 (0/3.3)	801.0 (0/1.7)	ν_{32} (e'')
		644.4 (0/5.5)			577.2 (0/1.3)	658.5 (0/4.0)	ν_{33} (e'')
		102.5 (0/0.0)			91.9 (0/0.3)	86.6 (0/0.1)	ν_{34} (e'')

Table 3. Comparison between observed and calculated (ZORA-BP86/I level of approximation) wavenumbers [cm^{-1}] for $M(C_2D_4)_3$ (M: Ni, Pd, and Pt) with the IR intensities [$km\,mol^{-1}$] and the Raman activities [$Å^4\,amu^{-1}$] of the calculated wavenumbers given in parentheses. Note that the experimental values refer exclusively to matrix-isolation experiments.

$[Ni(C_2D_4)_3]$			$[Pd(C_2D_4)_3]$			$[Pt(C_2D_4)_3]$	
IR	Raman	calcd	IR	Raman	calcd	calcd	assigned
		2229.0 (0/305.9)			2240.3 (0/186.7)	2231.6 (0/275.1)	ν_1 (a_1')
	1362	1343.4 (0/99.8)		1385	1362.8 (0/131.8)	1326.7 (0/79.5)	ν_2 (a_1')
	959	950.7 (0/31.0)			951.8 (0/26.8)	949.3 (0/24.2)	ν_3 (a_1')
	700	694.3 (0/13.4)			682.1 (0/9.1)	715.0 (0/17.2)	ν_4 (a_1')
	344	349.4 (0/21.7)		312	306.0 (0/28.8)	364.6 (0/25.3)	ν_5 (a_1')
		2192.5 (0/0)			2202.7 (0/0)	2198.6 (0/0)	ν_6 (a_2')
		1044.1 (0/0)			1048.5 (0/0)	1046.9 (0/0)	ν_7 (a_2')
		740.4 (0/0)			722.1 (0/0)	738.0 (0/0)	ν_8 (a_2')
		411.0 (0/0)			354.3 (0/0)	402.9 (0/0)	ν_9 (a_2')
		2229.8 (1.0/2.0)			2241.7 (0.0/5.4)	2232.8 (3.3/0.3)	ν_{10} (e')
2178	2178	2197.0 (39.7/85.5)			2204.6(23.7/37.7)	2201.4(33.1/76.1)	ν_{11} (e')
1362		1350.0 (52.8/25.9)	1378		1362.2(57.9/44.2)	1322.5(52.1/23.5)	ν_{12} (e')
		1051.4 (1.8/3.6)			1053.2 (1.4/3.1)	1052.1 (0.3/5.4)	ν_{13} (e')
952		943.1 (5.3/2.1)	951		946.1 (16.9/0.1)	938.9 (25.1/0.5)	ν_{14} (e')
		745.7 (0.7/0.2)			727.5 (0.0/0.7)	749.8 (2.2/0.5)	ν_{15} (e')
	683	681.3 (0.3/0.9)			658.3 (6.1/1.5)	675.2 (0.0/0.1)	ν_{16} (e')
		400.9 (24.1/4.9)			363.5 (0.1/12.1)	420.3 (0.0/21.1)	ν_{17} (e')
358		372.2 (41.5/8.6)			290.2 (37.9/0.4)	303.6 (33.0/3.1)	ν_{18} (e')
		206.4 (17.9/1.8)			136.0 (10.3/3.5)	127.1 (23.6/1.3)	ν_{19} (e')
		2311.8 (0/0)			2328.2 (0/0)	2322.6 (0/0)	ν_{20}(a_1'')
		949.1 (0/0)			953.5 (0/0)	947.1 (0/0)	ν_{21} (a_1'')
		664.2 (0/0)			664.7 (0/0)	658.6 (0/0)	ν_{22} (a_1'')
		82.4 (0/0)			100.9 (0/0)	95.3 (0/0)	ν_{23} (a_1'')
		2330.3 (23.6/0)			2342.7 (12.6/0)	2337.1 (15.2/0)	ν_{24} (a_2'')
		584.0 (0.9/0)			580.1 (0.0/0)	579.2 (0.8/0)	ν_{25} (a_2'')
		503.2 (1.4/0)			449.1 (0.2/0)	512.7 (0.5/0)	ν_{26} (a_2'')
		192.4 (0.1/0)			127.7 (0.5/0)	142.7 (1.7/0)	ν_{27} (a_2'')
		2327.9 (0/116.0)			2342.1 (0/81.5)	2336.5 (0/108.4)	ν_{28} (e'')
		2314.8 (0/88.9)			2327.9 (0/96.7)	2322.5 (0/102.6)	ν_{29} (e'')
		959.3 (0/0.5)			961.1 (0/1.8)	952.5 (0/2.0)	ν_{30} (e'')
		663.1 (0/2.2)			670.8 (0/0.3)	654.8 (0/0.1)	ν_{31} (e'')
		570.7 (0/0.1)			574.2 (0/0.8)	573.8 (0/0.2)	ν_{32} (e'')
		470.3 (0/4.9)			417.1 (0/1.6)	477.8 (0/3.8)	ν_{33} (e'')
		84.6 (0/0.1)			76.1 (0/0.4)	72.3 (0/0.1)	ν_{34} (e'')

Table 4. Wavenumbers for the coupled ν(C–C) and $\delta(CH_2)$ modes [cm^{-1}] for some C_2H_4 complexes.

Compound	ν(C–C)+$\delta(CH_2)$		Ref.
C_2H_4	1623	1342	
$[Li(C_2H_4)]$	1453[a]	1177	[39]
$[Al(C_2H_4)]$	1623	1340	[40]
$[In(C_2H_4)]$	1488	1201	[41]
$[Fe(C_2H_4)_2]$	1491[a]	1221(e)	[32]
$[Co(C_2H_4)]$	1504	1224	[33]
$[Co(C_2H_4)_2]$	1465	1222	[33]
$[Ni(C_2H_4)]$	1468	1166	[34]
$[Ni(C_2H_4)_3]$[b]	1512		[35]
$[Ni(C_2H_4)_3]$	1512/1516	1242 (IR/R)	[11,12]
$[Pd(C_2H_4)]$	1505	1216	[36]
$[Pd(C_2H_4)_3]$	1525/1531	1266/1256	this work
$[Pt(C_2H_4)_3]$[b]	1503/1501		[35]
$[Cu(C_2H_4)]$	1475	1156/1138 (IR)	[37]
$[Cu(C_2H_4)_2]$	1505	1228 (IR)	[37]
$[Cu(C_2H_4)_3]$	1525	1252	[37]
$[Ag(C_2H_4)]$	1476	1152/1132 (IR)	[38]
$[Au(C_2H_4)]$	1476	1144/1135 (IR)	[38]

[a] Calculated value on the basis of a force field. [b] Solutions in petroleum ether.

Table 4 do not agree in some cases. For example, the bond lengths in pm calculated by Alexander and Dines by using the B3LYP functional change in the order $[Fe(C_2H_4)]$ (143.5) < $[Co(C_2H_4)]$ (140.3) > $[Ni(C_2H_4)]$ (143.4) > $[Cu(C_2H_4)]$ (149.0 pm).[32] However, the experimentally observed wavenumbers of the stretching mode ν(C–C) follow the trend $[Co(C_2H_4)] > [Ni(C_2H_4)] < [Cu(C_2H_4)]$ (see Table 4). Calculations on the B3LYP level are not able to reproduce this trend in the wavenumbers, presumably because the mixing between ν(C–C) and $\delta(CH_2)$ is underestimated.[32] In summary, the accumulated data thus confirm, in agreement to earlier accounts, that the wavenumber of the $\nu_2(a)$ mode should not be taken as indicator of the bond strength.

In the case of uncoordinated C_2D_4, however, the mode coupling is reduced due to the relatively large energy separation.[24] The mode now assignable to a relatively pure C–C stretch occurs at 1515 cm^{-1}, and another one assignable to the CD_2 deformation occurs at 981 cm^{-1}. The signal at 1385 cm^{-1} in the Raman spectrum of $[Pd(C_2D_4)_3]$ is assigned to the ν(C–C) stretch, now significantly less mixed with the $\delta(CD_2)$ mode (the energy separation between the two modes is much larger). The corresponding signal for $[Ni(C_2D_4)_3]$ occurs at 1362 cm^{-1}. The signal at 951 cm^{-1} is due to the $\delta(CD_2)$ deformation, for which again the coupling with the ν(C–C) stretch is much smaller than for $[Pd(C_2H_4)_3]$. Finally, the signal at 312 cm^{-1} is attributable to the symmetric Pd–(C_2D_4) stretch. In the case of the $[Ni(C_2D_4)_3]$ complex, a signal at 344 cm^{-1} was assigned to the corresponding mode.

Very importantly, our spectra accumulated for $[Pd(C_2D_4)_3]$ show that the in-phase ν(C–C) mode, $\nu_2(a_1')$, is only slightly higher in energy (by 7 cm^{-1}) than the out-of-phase ν(C–C) mode, $\nu_{12}(e')$. In the case of the in-phase mode, the C···C distance between C atoms of adjacent C_2D_4 ligands decreases and increases to a maximum extent during the molecular motion. In the case of the out-of-phase C–C stretch the changes are smaller in total. The fact that the in-phase mode lies energetically above the out-of-phase mode is indicative of a small inter-ligand interaction. It is most likely

that a small repulsive interaction opposes shortening of the inter-ligand distance. There can, however, also be a small attractive interaction between the ligands which opposes an increase in the ligand–ligand distance. Such an attractive interaction would be in agreement with the "homoaromaticity" model as suggested by Herges and Papafilippopoulos.[4] However, the effect and thus the ligand–ligand interactions can only be extremely tiny. Otherwise, if larger interactions were present, the energetic difference between the two modes should be much larger. This difference $|\Delta\tilde{\nu}|$ (in cm^{-1}) correlates with the interaction force constant $f_{CC,CC}$ (in $N\,m^{-1}$) between two C_2D_4 ligands through Equation (1), where m_C is 12.01:[33]

$$\frac{\Delta\tilde{\nu}}{3} = 130.3\sqrt{\frac{2f_{CC,CC}}{m_C}} \qquad (1)$$

Applying Equation (1), the interaction constant, $f_{CC,CC}$, is approximately $0.002\,N\,m^{-1}$. For comparison, in 1,3-butadiene, the corresponding interaction force constant, as determined from a normal coordinate analysis, is $76\,N\,m^{-1}$.[34] This result strongly argues against any significant interligand interaction in $[Pd(C_2H_4)_3]$.

Charge density study: The spectroscopic results are supported by an analysis of the theoretical charge density distribution of the $[M(C_2H_4)_3]$ complexes (M = Ni **1**; Pd **2**; Pt **3**) (Figure 6). If not specified otherwise we will refer to the ZORA-BP86/TZ2P calculations as our default method in the following. The topology of the negative Laplacian, $L(\mathbf{r})$,[35] of the nickel species **1** in the molecular plane (Figure 6b) does not indicate any local charge accumulation between the individual ethylene ligands. In contrast, the valence shell charge concentration (VSCC) of the carbon atoms displays a locally increased charge accumulation pointing towards the nickel atom as illustrated in Figure 6b by arrows. These Ni–C-directed polarization features at the carbon atoms are opposed by three areas of increased Lewis acidity at the nickel atom in a key–lock type scenario (Figure 6b). In these areas the VSCC of the nickel atom is locally depleted. Topologically, these zones can be identified as (3,+1) critical points in the distribution of the negative Laplacian and are marked in Figure 6a as regions of charge depletion (CD) in the VSCC of nickel. As demonstrated by a combined experimental and theoretical charge density study of the electronically related monoethylene complex $[(C_2H_4)Ni(dbpe)]$ **4** (dbpe = 1,2-bis(di-*tert*-butylphosphino)-ethane), this polarization pattern of the charge density signals pronounced ethylene←Ni π back-donation.[36,37,38] We note, however, in contrast to the monoethylene complex **4**, that in the trisethylene complexes **1**–**3** two carbon atoms of neighboring ligands are sharing a single CD zone at the metal center. Hence, despite the absence of any significant direct interligand interactions all ligands are linked through a concerted key–lock scenario involving the three zones of charge depletion at the metal side.

The exocyclic curvature of the bond path at the Ni–C bond critical point (Figure 6b) indicates that the π component of the Dewar–Chatt–Duncanson (DCD) model[6] dominates the metal-to-ligand bonding in $[M(C_2H_4)_3]$.[39] Despite being weak, the presence of the corresponding DCD σ component is also revealed by a characteristic fingerprint displayed by the charge density distribution: The inwardly curved bond path in the valence regime of the carbon atoms is a clear hint for the presence of a noticeable ethylene→Ni σ donation.[36] Hence, the electronic structure of the $M(C_2H_4)_3$ complexes can basically be described by using the

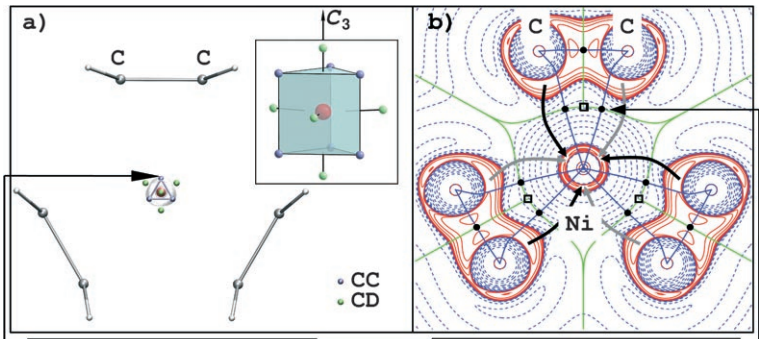

L_{CC} in eÅ^{-5}		
T	ZORA-BP86/I	BP86/II
Ni	1384	4044
Pd	240	833
Pt	–	652

ρ_{BCP} in eÅ^{-3}		
T	ZORA-BP86/I	BP86/II
Ni	0.60	0.57
Pd	0.53	0.52
Pt	0.63	0.63

Figure 6. a) Isovalue map of the negative Laplacian ($L(\mathbf{r}) = 1250\,e\,Å^{-5}$) of $[Ni(C_2H_4)_3]$ (BP86/III calculation). The insert shows the relative orientation of the five regions of local charge depletion (CD; marked by green spheres) and the six sites of local charge concentration (CC; blue spheres) in the valence-shell charge concentration (VSCC) of the nickel atom. The global polarization pattern of the nickel atom can be described by a trigonal prism the vertices of which are defined by the six CCs, whereas the faces denote the CD zones. Note that the magnitude of the charge concentrations in the isotypic $[M(\eta^2\text{-}C_2H_4)_3]$ complexes **1**–**3** decreases down the row Ni > Pd > Pt and is highly dependent on the level of approximation employed (**1** = 4044/1384/1332, **2** = 833/240, **3** = 652/– e Å^{-5}; BP86/II, and ZORA-BP86/I, and BP86/III (value solely for **1**) calculations, respectively); b) $L(\mathbf{r})$ contour maps; the arrows illustrate the key–lock scenario displayed by the polarized VSCC at the carbon atoms and the charge-depletion (CD) zones at the central Ni atom in the molecular plane. Default contour levels are drawn at 0.0, $\pm 2.0\times10^n$, $\pm 4.0\times10^n$, $\pm 8.0\times10^n$ e Å^{-5}, where $n = 0, \pm3, \pm2, \pm1$; extra level at 900 and 1000 e Å^{-5}; the contour line at 800 e Å^{-5} is omitted for clarity; positive and negative values are marked by —— and – – – lines, respectively. BCPs and RCPs are marked by ● and □, respectively; the bond paths are shown by solid lines.

classical DCD model. No evidence can be found for the presence of homoaromaticity.

This is further supported by the delocalization indices[40] and the topological parameters of the C–C bond critical points. We first note that the topology of the charge density at the C–C bond critical points of the $[M(C_2H_4)_3]$ complexes remains rather invariant with respect to metal substitution (Table 5). The trend to reduced bond ellipticities across the series **1**>**2**>**3** (ε = 0.25 (Ni) > 0.24 (Pd) > 0.22 (Pt)) suggests that a metallacyclopropane character, as an alternative to the DCD picture, might become more important for the platinum complex **3** than for its first- and second-row transition-metal congeners **1** and **2**. In line with this argument, **3** shows the most pronounced M–C bond path of the tris(ethylene)s as suggested by the smallest bond path ellipticity (ε = 1.70 (Ni); 2.02 (Pd); 1.06 (Pt)). Hence, in direct comparison with the theoretical benchmark ethylene **5** and benzene **6** (C–C bond orders (BO) of 2 and 1.5, respectively), we find a significantly reduced double-bond character in all tris-ethylenes: BO = 1.47, 1.52, and 1.41 for **1**, **2**, and **3**, respectively. In comparison with the experimental benchmarks for mono- and tetra-olefin complexes **4** and $[Ni(cod)_2]$ (cod = 1,5-cyclooctadiene)[36,39] **7** displaying bond orders of 1.56 and 1.61, respectively, we might conclude that the C–C bonding characteristics in **1**–**3** do not show any unexpected behavior.[41] This classification is also supported by computed electron delocalization indices for the C–C bond ($\delta(\Omega,\Omega')_{C-C}$ = 1.374/1.389 for **1** and **6**, respectively) which do not differ significantly. On the contrary, for the hypothetical C···C interligand interaction only a rather low delocalization index ($\delta(\Omega,\Omega')_{C\cdots C}$ = 0.139) is calculated ruling out any significant covalent character.

We were motivated to compare the chemical reactivities because of the topological similarity of the charge distribution in **1** and our experimental benchmark **4**. In the following we have therefore analyzed changes in electronic structure of these textbook examples of neutral d^{10} nickel ethylene complexes on protonation. As demonstrated by Spencer and co-workers[42] earlier the β-agostic cationic nickel d^8 species $[EtNi(dbpe)][BF_4]$ **4**$[H^+]$ evolves from **4** when HBF_4 is employed as protonation reagent. In the case of **1** the same reaction behavior is predicted by our quantum-chemical calculations leading to the protonated version of the trisethylene species **1**$[H^+]$. Analysis of the topology of the theoretical charge density of **1**$[H^+]$ (Figure 7) highlights a simple rule: The agostic hydrogen atom faces a zone of locally increased Lewis acidity in the valence shell of the transition-metal atom. Hence, the C–H bond activation is controlled by the local Lewis acidity of the transition-metal atom in **1**$[H^+]$.[43,44] The protonation step occurs in both cases, **1** and **4**, according to the calculations without any significant energy barrier. Hence, also from a chemical point of view **1** does not display any additional homoaromatic energy stabilization relative to our mono-ethylene complex **4**.

Table 5. ZORA-BP86/I analysis of bond and ring critical points in **1**–**6**; $\rho(\mathbf{r})$ is given in e Å^{-3}, $\nabla^2\rho(\mathbf{r})$ in e Å^{-5}; all lengths in Å.

		4[a]	**1**	**2**	**3**	**7**[b]	**5**	**6**
C–C	distance	1.4189(6)	1.394	1.389	1.406	1.391(2)	1.333	1.398
	$\rho(\mathbf{r}_b)$	2.107(9)	2.055	2.085	2.018	2.137(7)	2.330	2.075
	ε	0.25	0.25	0.24	0.22	0.180(1)	0.30	0.18
	$\nabla^2\rho(\mathbf{r}_b)$	−20.88(3)	−19.0	−19.7	−18.5	−20.8(1)	−24.3	−20.0
T–C	distance	1.9708(4) 1.9715(4)	2.043	2.222	2.194	2.130(9) 2.117(3)	–	–
	$\rho(\mathbf{r}_b)$	0.671(6) 0.670(2)	0.600	0.533	0.632	0.548(7) 0.543(4)	–	–
	ε	1.03 1.05	1.70	2.02	1.06	2.5(3) 5.1(3)	–	–
	$\nabla^2\rho(\mathbf{r}_b)$	8.393(13) 8.392(6)	5.4	4.9	4.4	4.98(4) 5.39(7)	–	–
[TC_2] RCP	$\rho(\mathbf{r}_r)$	0.648	0.588	0.525	0.610	[b]	–	–
	$\nabla^2\rho(\mathbf{r}_r)$	8.9	6.8	5.9	5.9	[b]	–	–

[a] Experimental data (two independent Ni–C distances), see ref. [36] [b] Experimental data (two independent Ni–C distances), according to ref. [39] a ring critical point (RCP) has been located in the center of each of the four rings; $\nabla^2\rho(\mathbf{r}_r)$ is positive; $\rho(\mathbf{r}_r)$ is very similar to the two corresponding bond critical points $\rho(\mathbf{r}_b)$ values ($\Delta[\rho(\mathbf{r}_b)-\rho(\mathbf{r}_r)]$ = 0.01–0.03 e Å^{-3}).

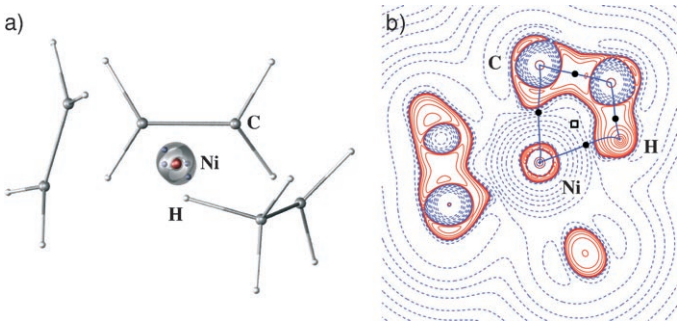

Figure 7. a) Molecular structure of the protonated species $[EtNi(\eta^2\text{-}C_2H_4)_2]^+$ **1**$[H^+]$ as obtained from the BP86/III calculations and $L(\mathbf{r})$ = 1100 e Å^{-5} isovalue map. The agostic hydrogen atom is facing a valence charge depletion (CD) zone at the central Ni atom in the plane spanned by the agnostic Ni,C,C,H moiety. b) $L(\mathbf{r})$ contour maps and molecular graph displaying a pronounced Ni···H bond path in the molecular plane. Default contour levels as specified in Figure 6b), except for the extra contours at 1200 and 1500 e Å^{-5}.

Conclusion

To summarize, the Raman and IR spectra accumulated for $[Pd(C_2H_4)_3]$ can be used to estimate the interaction between adjacent C_2H_4 ligands in the complex. The interaction force constant $f_{CC,CC}$ turns out to be 0.002 N m^{-1} (for comparison, 76 N m^{-1} in butadiene). Analysis of the topology of the charge density distribution and evaluation of electron delocalization indices do not provide evidence for any significant interligand interaction in combination with a homoaromatic stabilization.[45] In contrast, the remarkable stability of these

trisolefin complexes can be described in the framework of the classical Dewar–Chatt–Duncanson model. Solely in the case of the platinum compound the alternative metallacyclopropane bonding description becomes more important. These findings are supported by the predicted chemical behavior of **1**–**3** on protonation. As in the case of the d^{10}-configured mono-ethylene species of Group 10 elements, protonation leads directly to the agostic mono-alkyl species $[EtM(\eta^2\text{-}C_2H_4)_2]^+$. Hence, we cannot find any indication (on the basis of observable physical or chemical properties) which supports the presence of relevant homoaromaticity in these tris(ethylene) complexes. Accordingly, our study is in clear contrast to the earlier suggestions by Herges and co-workers.[4]

Experimental Details

Pd was evaporated by resistively heating a Pd filament (Chempur, purity 99.95%, 0.25 mm diameter) in a high-vacuum apparatus. The Pd vapor was codeposited together with pure C_2H_4 (Messer, purity 99.95%) for the Raman experiments and with up to 10% C_2H_4 in Ar (Messer, purity 99.998%) for the IR experiments onto a Cu surface cooled to 12 K by using a closed-cycle refrigerator (Leybold LB510). Further details about the matrix-isolation technique can be found elsewhere.[46] The experiments were repeated with C_2D_4 (Sigma–Aldrich, purity 99%).

Raman spectra were recorded at a resolution of 0.5 cm^{-1} by using an XY spectrometer from Jobin–Yvon equipped with a triple-monochromator and a CCD camera detector. The $\lambda = 488$ nm line of an Ar^+ laser was used to excite the molecules. Raman spectra were measured without polarization of the laser light. An IFS 113v IR spectrometer from Bruker was used to measure the IR spectra. Spectra in the region 400–4000 cm^{-1} were recorded at a resolution of 0.1 cm^{-1} with a MCT detector; spectra in the region 200–700 cm^{-1} were measured by using a DTGS detector working at a resolution of 0.2 cm^{-1}.

It should be mentioned that the difference between some of the modes that were detected in our study for the first time was so small (less than 10 cm^{-1}) that the two modes could not be distinguished in the vibrational spectra of the molecule as measured by routine methods (solid material or solution, even at −50 °C, as well as any KBr disc or Nujol suspension data). The advantage of the matrix-isolation technique is that the rotations of the molecules in the matrix environment are quenched so that purely vibrational bands/signals result exhibiting generally a small half-width. In addition, hot bands are also absent due to the low temperature of around 10 K. On the other hand of course, the matrix-isolation technique has the disadvantage of producing only small amounts of the desired molecule so that intensity can be a problem.

Computational details: The molecular geometries of $[Ni(C_2H_4)_3]$, $[Pd(C_2H_4)_3]$, and $[Pt(C_2H_4)_3]$ were optimized in D_{3h} symmetry by using ADF[47,48,49,50] employing the gradient-corrected BP86 density functional[51] and the TZ2P basis as implemented in ADF. The two-component ZORA Hamiltonian was used to include relativistic effects. This method will be denoted ZORA-BP86/I in the following. Note that the optimized geometries were kept fixed during the subsequent charge density studies to ensure that the interpretation of the results was not affected by deviating molecular structures. Vibrational normal modes and frequencies were calculated from analytical energy gradients within ADF. IR intensities and Raman activities [Eq. (2)]

$$S_p = 45a'^2_p + 7\gamma'^2_p \quad (2)$$

where a'^2_p and γ'^2_p contain the derivatives of the polarizability components with respect to a given normal coordinate p, were obtained from the program SNF.[52]

We compared the topology of the electron density distribution, $\rho(\mathbf{r})$, obtained by two different approaches: 1) BP86/II-(effective-core-potential)-type calculations by using the Stuttgart quasirelativistic small-core effective core potentials (ECPs), (RSC 1997 ECP; 28 electrons)[53] for the metals and standard 6-311G(d,p)[54] bases for the remaining atoms as implemented in Gaussian 03[55] and; 2) the quasirelativistic all-electron ZORA-BP86/I model. In the case of the ADF calculations, numerical analyses of density grid files were performed by using the INTEGRITY program by P. Rabillier[56] and the program DGrid by M. Kohout.[57] Finally, the topology of $\rho(\mathbf{r})$ of $[Ni(C_2H_4)_3]$ and $[EtNi(\eta^2\text{-}C_2H_4)_2]^+$ was analyzed analytically at: 3) the BP86/III level of approximation employing 6-311G(d,p) bases as implemented in Gaussian 03 and a local version of the AIMPAC software package[58] for the evaluation of Gaussian wavefunction files. Delocalization indices were calculated at the same level by using the AIMDELOC01 script developed by C. F. Matta[59] and an approximation suggested by J. Poater and co-workers.[60]

Acknowledgements

The authors gratefully acknowledge financial support from the DFG-Schwerpunktprogramm SPP1178 of the Deutsche Forschungsgemeinschaft the Fonds der Chemischen Industrie, and by Nanocat, an International Graduate Program within the Elitenetzwerk Bayern.

[1] See, for example: a) S. M. Pillai, M. Ravindranathan, S. Sivaram, *Chem. Rev.* **1986**, *86*, 353–399; b) S. D. Ittel, L. K. Johnson, M. Brookhart, *Chem. Rev.* **2000**, *100*, 1169–1204, and references therein.

[2] a) K. Fischer, K. Jonas, G. Wilke, *Angew. Chem.* **1973**, *85*, 620–621; *Angew. Chem. Int. Ed. Engl.* **1973**, *12*, 565–566; b) K. Fischer, K. Jonas, P. Misbach, R. Stabba, G. Wilke, *Angew. Chem.* **1973**, *85*, 1002–1012; *Angew. Chem. Int. Ed. Engl.* **1973**, *12*, 943–953.

[3] N. Roesch, R. Hoffmann, *Inorg. Chem.* **1974**, *13*, 2656–2666.

[4] R. Herges, A. Papafilippopoulos, *Angew. Chem.* **2001**, *113*, 4809–4813; *Angew. Chem. Int. Ed.* **2001**, *40*, 4671–4674.

[5] I. Krossing, A. Reisinger, *Angew. Chem.* **2003**, *115*, 5903–5906; *Angew. Chem. Int. Ed.* **2003**, *42*, 5725–5728.

[6] a) M. J. S. Dewar, *Bull. Soc. Chim. Fr.* **1951**, *18*, C71–C79; b) J. Chatt, L. A. Duncanson, *J. Chem. Soc.* **1953**, 2939–2947.

[7] See, for example the discussion in the case of M-N_2 complexes in: H.-J. Himmel, M. Reiher, *Angew. Chem.* **2006**, *118*, 6412–6437; *Angew. Chem. Int. Ed.* **2006**, *45*, 6264–6288.

[8] M. Green, J. A. K. Howard, J. L. Spencer, F. G. A. Stone, *J. Chem. Soc. Dalton Trans.* **1977**, 271–277.

[9] M. Green, J. A. K. Howard, J. L. Spencer, F. G. A. Stone, *J. Chem. Soc. Chem. Commun.* **1975**, 449–451.

[10] a) G. H. van Nes, A. Vos, *Acta Crystallogr. Sect. B* **1979**, *35*, 2593–2594; b) J. L. Duncan, D. C. McKean, P. D. Mallinson, *J. Mol. Spectrosc.* **1973**, *45*, 221–246.

[11] H. Huber, G. A. Ozin, W. J. Power, *J. Am. Chem. Soc.* **1976**, *98*, 6508–6511.

[12] T. Merle-Mejean, C. Cosse-Mertens, S. Bouchareb, F. Galan, J. Mascetti, M. Tranquille, *J. Phys. Chem.* **1992**, *96*, 9148–9158.

[13] a) G. A. Ozin, D. F. McIntosh, W. J. Power, R. P. Messmer, *Inorg. Chem.* **1981**, *20*, 1782–1792; b) E. S. Kline, Z. H. Kafafi, R. H. Hauge, J. L. Margrave, *J. Am. Chem. Soc.* **1987**, *109*, 2402–2409.

[14] H. Huber, D. McIntosh, G. A. Ozin, *Inorg. Chem.* **1977**, *16*, 979–983.

[15] J. A. K. Howard, J. L. Spencer, S. A. Mason, *Proc. R. Soc. London Ser. A* **1983**, *386*, 145–161.

[16] A series of experiments has been carried out in which the concentration of both ethylene and Pd has been varied. Experiments with 0.1–2% C_2H_4 gave evidence for bands belonging to the monoethylene and bis(ethylene) complexes $[PdC_2H_4]$ and $[Pd(C_2H_4)_2]$. For increased concentrations, $[Pd(C_2H_4)_3]$ was detected as the dominating

product. For that reason we have used high concentrations of ethylene in our experiments. For all bands/signals assigned to $[Pd(C_2H_4)_3]$ the relative intensities were observed to remain unchanged in all experiments with different conditions (change of concentrations and annealing experiments). The Raman spectra were recorded in pure C_2H_4. In this environment we observed only signals from $[Pd(C_2H_4)_3]$. No signals assignable to a product between Pd dimers or clusters and C_2H_4 were visible in the spectra, even for increased Pd concentrations.

[17] a) J. L. Duncan, E. Hamilton, *J. Mol. Spectrosc.* **1981**, *76*, 65–60; b) Z. H. Kafafi, R. H. Hauge, J. L. Margrave, *J. Am. Chem. Soc.* **1985**, *107*, 7550–7559.

[18] A. J. L. Hanlan, G. A. Ozin, W. J. Power, *Inorg. Chem.* **1978**, *17*, 3648–3657.

[19] Y. K. Lee, Y. Hannachi, C. Xu, L. Andrews, L. Manceron, *J. Phys. Chem.* **1996**, *100*, 11228–11234.

[20] P. Csaszar, P. L. Goggin, J. L. Spencer, *J. Organomet. Chem.* **1989**, *379*, 337–349.

[21] H.-G. Cho, L. Andrews, *J. Phys. Chem. A* **2004**, *108*, 6272–6278.

[22] a) H. Huber, D. McIntosh, G. A. Ozin, *J. Organomet. Chem.* **1976**, *112*, C50–C54; b) G. A. Ozin, H. Huber, D. McIntosh, *Inorg. Chem.* **1977**, *16*, 3070–3078.

[23] D. McIntosh, G. A. Ozin, *J. Organomet. Chem.* **1976**, *121*, 127–136.

[24] L. Manceron, L. Andrews, *J. Phys. Chem.* **1986**, *90*, 4514–4528.

[25] L. Manceron, L. Andrews, *J. Phys. Chem.* **1989**, *93*, 2964–2970.

[26] L. Manceron, L. Andrews, *J. Phys. Chem.* **1990**, *94*, 3513–3518.

[27] G. Maier, H. P. Reisenauer, H. Egenolf, *Eur. J. Org. Chem.* **1998**, 1313–1317.

[28] a) P. H. Kasai, C. McLeod, T. Watanabe, *J. Am. Chem. Soc.* **1980**, *102*, 179–190; b) J. A. Howard, H. A. Joly, B. Mille, *J. Phys. Chem.* **1990**, *94*, 1275–1279.

[29] R. Grinter, S. J. Stotesbury, *J. Mol. Struct.* **1982**, *80*, 125–128.

[30] Y. K. Lee, L. Manceron, I. Pápai, *J. Phys. Chem. A* **1997**, *101*, 9650–9659.

[31] P. Csaszar, P. L. Goggin, J. Mink, J. L. Spencer, *J. Organomet. Chem.* **1989**, *379*, 337–349.

[32] B. D. Alexander, T. J. Dines, *J. Phys. Chem. A* **2004**, *108*, 146–156.

[33] We neglect the coupling between the ν(C–C) stretch and other vibrations in the complex. As already mentioned, this is a working approximation in the case of C_2D_4, but not C_2H_4, because the ν(C–C) stretch couples heavily with the deformation mode $\delta(CH_2)$ in C_2H_4. If we neglect the coupling, we simply have a two-center problem and the relation between the harmonic frequency and the force constant is given by Hook's law, if we neglect in addition any anharmonicity effects. If the three C_2H_4 moieties would not interact (interaction force constant equals zero), we would observe a single band due to the ν(C–C) stretch for the complex (all C–C stretches have similar energy). The interaction causes the three stretches to appear at different wavenumbers in the spectra. In the D_{3h} symmetry of the complex the three coupled C–C stretches belong to the irreducible representations a_1' and e'. In our special case, the a_1' mode turns out to be higher in energy than the e' mode. The e' contains two vibrations. The e' mode is found at an energy which is lower than the energy of uncoupled C–C oscillators and the a_1' mode is found at a higher energy. However, in total the energy increase and decrease relative to the uncoupled case should be zero in our simple model. Therefore the energy difference between the a_1' mode and the hypothetical position in the case of noncoupling C–C oscillators is two times larger than the difference between the e' mode and the hypothetical position of noncoupling C–C oscillators. The symmetry force constants amount to $f_{CC}+2f_{CC,CC}$ and $f_{CC}-f_{CC,CC}$ for the a_1' and the e' mode. A third of the difference between the wavenumbers observed for the a_1' and the e' modes is therefore related to the $f_{CC,CC}$ interaction force constant. Given that the relation is approximately described by Hook's law we immediately obtain Equation (1).

[34] K. B. Wiberg, R. E. Rosenberg, *J. Am. Chem. Soc.* **1990**, *112*, 1509–1519.

[35] R. F. W. Bader and co-workers have demonstrated that the negative Laplacian of the charge density distribution, $L(\mathbf{r}) = -\nabla^2\rho(\mathbf{r})$, determines where the charge density distribution is locally concentrated ($L(\mathbf{r})>0$) or locally depleted ($L(\mathbf{r})<0$). Accordingly, the $L(\mathbf{r})$ function can be employed to resolve the shell structure for elements with $Z \leq 18$. However, the shell structure of the transargonic elements is not fully represented by the Laplacian. In general the fourth, fifth, or sixth shell for elements of Periods 4–6, respectively, is not revealed in the Laplacian. As a convention Bader and coworkers suggested that the outermost shell of charge concentration (CC) of an atom (*second* shell of CC of the carbon atoms and *third* shell of CC of the nickel atom) represents its (effective) valence shell charge concentration (VSCC). a) R. F. W. Bader, P. J. MacDougall, C. D. H. Lau, *J. Am. Chem. Soc.* **1984**, *106*, 1594–1605; b) R. F. W. Bader, H. Essén, *J. Chem. Phys.* **1984**, *80*, 1943–1960; c) R. P. Sagar, A. C. T. Ku, V. Smith, *J. Chem. Phys.* **1988**, *88*, 4367–4374; d) Z. Shi, R. J. Boyd, *J. Chem. Phys.* **1988**, *88*, 4375–4377; e) W.-T. Chan, I. P. Hamilton, *J. Chem. Phys.* **1998**, *108*, 2473–2485; f) M. Kohout, A. Savin, H. Preuss, *J. Chem. Phys.* **1991**, *95*, 1928–1933; g) R. F. W. Bader, R. J. Gillespie, F. Martín, *Chem. Phys. Lett.* **1998**, *290*, 488–494.

[36] W. Scherer, G. Eickerling, D. Shorokov, E. Gullo, G. S. McGrady, P. Sirsch, *New J. Chem.* **2006**, *30*, 309–312.

[37] As illustrated by Figure 6 the magnitude of the ligand-induced charge concentrations (LICCs) significantly decreases down the group Ni > Pd > Pt. From simple chemical considerations we suggest that LICCs of *n*d metals of the same group critically depend on two (counteracting) factors: 1) The polarizabilitiy of the valence density and; 2) the expansion of the valence shell. In the case of first-row transition metals the 3d functions are less diffuse and less polarizable relative to the 4d or the 5d metals. However, the magnitude of the LICCs is at maximum for 3d metals due to the fact that electron–electron repulsion and spin correlation is at a maximum for the 3d metals as a consequence of the more contracted valence shell compared with the 4d and 5d metals. Thus, the second factor appears to be dominant and thus leads to a more pronounced electron localization in the form of larger charge concentrations in the case of 3d versus 4d, or 5d metals. For a general discussion of the chemical nature of LICCs see: G. S. McGrady, A. Haaland, H. P. Verne, H. V. Volden, A. J. Downs, D. Shorokhov, G. Eickerling, W. Scherer, *Chem. Eur. J.* **2005**, *11*, 4921–4934.

[38] We note that the LICCs of **3** are not resolved as (3, −3) critical points in the negative Laplacian by the ZORA-BP86/I calculations in contrast to the BP86/II calculations. A similar result was however obtained earlier by fully relativistic, so-called four-component calculations on spherical symmetric atoms (Au) by Kohout and co-workers (ref. [35 f]) These authors already found that the two outermost shells of an atom of the 6th period are not resolved in the second derivative of the radial density. We note, however, that deletion of the 4f contributions to the total ZORA-BP86/I charge density in **3** regenerates the polarization pattern obtained by using the BP86/II calculations based on semirelativistic small-core ECPs. Also isosurface maps of the electron localizability indicator (ELI) as defined by M. Kohout (see for example: M. Kohout, *Faraday Discuss.* **2007**, *135*, 43–54) recover the polarization pattern given by BP86/II calculations on the basis of the ZORA-BP86/I calculations. Hence, the complexes **1**–**3** show the same polarization of the valence density.

[39] P. Macchi, D. M. Proserpio, A. Sironi, *J. Am. Chem. Soc.* **1998**, *120*, 1447–1455.

[40] X. Fradera, M. A. Austen, R. F. W. Bader, *J. Phys. Chem. A* **1999**, *103*, 304–314.

[41] The bond orders were derived by using the empirical formula $n = \exp\{A[\rho(\mathbf{r}_b)-B]\}$ (see: R. F. W. Bader, Atoms in *Molecules: A Quantum Theory; International Series of Monographs on Chemistry, Vol 22*, Oxford University Press, Oxford, **1990**). *A* and *B* are parameters that were adjusted to fit the bond orders of $n = 1.5$ and 2 of benzene and ethylene, respectively, on the basis of the charge densities at the bond critical points, $\rho(\mathbf{r}_b)_{C-C}$, at the ZORA-BP86/I level of theory. In the case of **4** and **7**, the experimental $\rho(\mathbf{r}_b)_{C-C}$ values were employed.

[42] F. M. Conroy-Lewis, L. Mole, A. D. Redhouse, S. A. Litster, J. L. Spencer, *J. Chem. Soc. Chem. Commun.* **1991**, 1601–1603.
[43] The same topological scenario is also shown by our experimental benchmark system **4**[H^+] (W. Scherer, S. Altmannhofer, V. Herz, unpublished results).
[44] A similar rule was already found in the case of agostic d^0 transition-metal alkyls: a) W. Scherer, P. Sirsch, D. Shorokhov, M. Tafipolsky, G. S. McGrady, E. Gullo, *Chem. Eur. J.* **2003**, *9*, 6057–6070; b) W. Scherer, G. S. McGrady, *Angew. Chem.* **2004**, *116*, 1816–1842; *Angew. Chem. Int. Ed.* **2004**, *43*, 1782–1806. However, in contrast to the electron-rich agostic d^8 complexes the highly Lewis acidic d^0 congeners are characterized by the fact that the activated C–H bond (and not the agostic hydrogen atom itself) is facing a local Lewis acidic center at the transition-metal center. We suggest that this difference between agostic d^0 and d^8 species is reflecting the fact that in the electron-rich complexes **1**[H^+] and **4**[H^+] the C–H bond activation is much more pronounced (>10 pm) than in the case of typical electron-poor d^0 congeners (<5 pm) or main-group compounds like lithium alkyls (<1 pm); c) W. Scherer, P. Sirsch, D. Shorokhov, G. S. McGrady, S. A. Mason, M. G. Gardiner, *Chem. Eur. J.* **2002**, *8*, 2324–2334; d) W. Scherer, P. Sirsch, M. Grosche, M. Spiegler, S. A. Mason, M. G. Gardiner, *Chem. Commun.* **2001**, 2072–2073. Hence the hydridic character of the agostic hydrogen atom becomes dominant in **1**[H^+] and **4**[H^+].
[45] The shortest C···C distances between C atoms of adjacent ethylene ligands in the complexes $[M(C_2H_4)_3]$ of 262.9 (Ni), 296.2 (Pd), and 289.6 pm (Pt) also argue against a significant through-space interaction. It has been shown for many organic molecules containing non-conjugated π systems that such an interaction is hardly present for distances exceeding 250 pm. See, for example: R. Gleiter, W. Schäfer, *Acc. Chem. Res.* **1990**, *23*, 369–375.
[46] See, for example: a) Chemistry and Physics of Matrix-Isolated Species (Eds.: L. Andrews, M. Moskovits), North Holland, Amsterdam, **1989**; b) I. R. Dunkin, Matrix-Isolation Techniques: A Practical Approach, Oxford University Press, Oxford, **1998**; c) H.-J. Himmel, A. J. Downs, T. M. Greene, *Chem. Rev.* **2002**, *102*, 4191–4242.
[47] G. te Velde, F. M. Bickelhaupt, S. J. A. van Gisbergen, C. Fonseca Guerra, E. J. Baerends, J. G. Snijders, T. Ziegler, *J. Comput. Chem.* **2001**, *22*, 931–967.
[48] C. Fonseca Guerra, J. G. Snijders, G. te Velde, E. J. Baerends, *Theor. Chem. Acc.* **1998**, *99*, 391–403.
[49] ADF2005.01, SCM, Theoretical Chemistry, Vrije Universiteit Amsterdam, The Netherlands, http://www.scm.com.
[50] E. van Lenthe, A. E. Ehlers, E. J. Baerends, *J. Chem. Phys.* **1999**, *110*, 8943–8953.
[51] a) A. D. Becke, *Phys. Rev. A* **1988**, 38, 3098–3100; b) J. P. Perdew, *Phys. Rev. B* **1986**, *33*, 8822–8824.
[52] J. Neugebauer, M. Reiher, C. Kind, B. A. Hess, *J. Comput. Chem.* **2002**, *23*, 895–910.
[53] a) D. Andrae, U. Haeussermann, M. Dolg, H. Stoll, H. Preuss, *Theor. Chim. Acta* **1990**, *77*, 123–141; b) M. Dolg, U. Wedig, H. Stoll, H. Preuss, *J. Chem. Phys.* **1987**, *86*, 866–872.
[54] R. Krishnan, J. S. Binkley, R. Seeger, J. A. Pople, *J. Chem. Phys.* **1980**, *72*, 650–654.
[55] Gaussian 03 (Revision B.03), M. J. Frisch, G. W. Trucks, H. B. Schlegel, G. E. Scuseria, M. A. Robb, J. R. Cheeseman, J. A. Montgomery, Jr., T. Vreven, K. N. Kudin, J. C. Burant, J. M. Millam, S. S. Iyengar, J. Tomasi, V. Barone, B. Mennucci, M. Cossi, G. Scalmani, N. Rega, G. A. Petersson, H. Nakatsuji, M. Hada, M. Ehara, K. Toyota, R. Fukuda, J. Hasegawa, M. Ishida, T. Nakajima, Y. Honda, O. Kitao, H. Nakai, M. Klene, X. Li, J. E. Knox, H. P. Hratchian, J. B. Cross, V. Bakken, C. Adamo, J. Jaramillo, R. Gomperts, R. E. Stratmann, O. Yazyev, A. J. Austin, R. Cammi, C. Pomelli, J. W. Ochterski, P. Y. Ayala, K. Morokuma, G. A. Voth, P. Salvador, J. J. Dannenberg, V. G. Zakrzewski, S. Dapprich, A. D. Daniels, M. C. Strain, O. Farkas, D. K. Malick, A. D. Rabuck, K. Raghavachari, J. B. Foresman, J. V. Ortiz, Q. Cui, A. G. Baboul, S. Clifford, J. Cioslowski, B. B. Stefanov, G. Liu, A. Liashenko, P. Piskorz, I. Komaromi, R. L. Martin, D. J. Fox, T. Keith, M. A. Al-Laham, C. Y. Peng, A. Nanayakkara, M. Challacombe, P. M. W. Gill, B. Johnson, W. Chen, M. W. Wong, C. Gonzalez, J. A. Pople, Gaussian, Inc., Wallingford CT, **2004**.
[56] C. Katan, P. Rabillier, C. Lecomte, M. Guezo, V. Oison, M. Souhassou, *J. Appl. Crystallogr.* **2003**, *36*, 65–73.
[57] M. Kohout, Program DGrid 4.1, Max Planck Institute for Chemical Physics of Solids, Dresden, **2006**.
[58] F. W. Biegler-König, R. F. W. Bader, T. Tang, *J. Comput. Chem.* **1982**, *3*, 317–328.
[59] C. F. Matta, AIMDELOC01, QCPE0802, QCPE, Indiana University, Indiana (USA), **2001**.
[60] J. Poater, M. Solà, M. Duran, X. Fradera, *Theor. Chim. Acta* **2002**, *107*, 362–371. According to Poater and co-workers the delocalization indices $\delta(\Omega,\Omega')$ of DFT wavefunctions can be calculated by using an approximate formula that makes use of an HF-like second-order exchange density matrix. According to a recent study by C. Gatti and co-workers (C. Gatti, D. Lasi, *Faraday Discuss.* **2007**, *135*, 55–78) this approximation affords $\delta(\Omega,\Omega')$ values which are, not surprisingly, very close to those of HF, although it erroneously implies that the electron-pair density matrix can be constructed, within DFT, by using the same simple formalism valid for the HF method.

Received: June 12, 2007
Published online: September 28, 2007

